FFEMS Fatigue & Fracture of Engineering Materials & Structures

doi: 10.1111/ffe.12130

Computational fretting fatigue maps for different plasticity models

M. ALQUEZAR[1], V. ARRIETA[1], A. CONSTANTINESCU[2], L. FLANDI[2], M. H. MAITOURNAM[2] and P. WACKERS[1]

[1]*Laboratoire de Mécanique des Solides, Department of Mechanics - Ecole Polytechnique, - CNRS, Palaiseau, France,* [2]*Structural Mechanics, Blades-Vanes and Casing (TESB), MTU Aero Engines GmbH, Muenchen, Germany*

Received Date: 25 April 2013; Accepted Date: 4 November 2013; Published Online: 9 January 2013

ABSTRACT This paper presents qualitative elastoplastic simulations and analyses of fretting fatigue. Three hardening constitutive models are considered, and their effects on stick–slip conditions and lifetime prediction are compared. The computational analysis consists of the estimation of the shakedown limit cycle and the fatigue prediction using Dang Van or Crossland criterion. A particular configuration, the interaction of a flat pad with rounded corners in contact with a flat substrate made, respectively, of Inconel In718 and Titanium Ti64 alloys, is studied. The shakedown state is analysed using the cyclic and ratcheting equivalent strain concepts already discussed in the literature.

In the paper, different fretting maps, based on slip, shakedown and fatigue regimes, are numerically produced and analysed. A new variable, the global slip percentage, is proposed for the characterization of the stick–slip regimes. Analyses of a series of slip maps show that the different hardening models do not introduce significant changes in the stick–slip conditions. Using finite element method simulations combined with fatigue limit criteria (Dang Van and Crossland), fretting fatigue maps are qualitatively reproduced. The main contribution of this work is a comparative discussion on the influence of the hardening models complexity on such maps.

Keywords fatigue; finite elements; fretting; friction; shakedown; slip; stick.

NOMENCLATURE

$a_N^{(i)}, b_N^{(i)}$ = material parameters for lifetime at N cycles for criterion (i)
ES = elastic shakedown
p = surface contact pressure
PS = plastic shakedown
q = shear stress
RA = ratcheting
ε = strain tensor
ε_c = cyclic strain
ε_r = ratcheting strain
ε_Y = yield strain
σ = stress tensor
σ_Y = yield stress

INTRODUCTION

Fretting fatigue is associated with small cyclic tangential movements between two surfaces in contact. The underlying damage mechanisms are activated by the complex pressure and tangential surface tractions acting along the surfaces in frictional contact.

Correspondence: A. Constantinescu. E-mail: andrei.constantinescu@lms.polytechnique.fr

Fretting fatigue is a serious engineering problem in different structural components: bolts, rivets, turbine blade fixings, bearings and so on. It has therefore attracted the attention of engineers and researchers for decades. The difficulty of the problem lies in the large number of parameters, the length scales involved and the nonlinearity induced by the frictional contact and materials behaviour.

The experimental work in this field has shown the practical importance of the so-called fretting maps[1,2] (for recent discussions and applications, see, e.g[3,4]). The

fretting maps display the cyclic regime in terms of the applied vertical force and the tangential displacement. The nonlinear regime is qualified in terms of global elastic or plastic shakedown (PS) or in terms of stick or slip to characterize the state of the surfaces in contact. It permits to establish a relation with fretting or wear damage.

The classical attempt to model this problem is based on closed-form expressions for the strain and stress fields obtained in the special configurations of elastic bodies in contact. An extended presentation of closed-form solutions is given in Refs [5,6]. Examples of recent developments of these techniques are the results presented in Refs [7–9] where crack type singular fields describe the stress field at the corner of the fretting pad or as in Ref. [10] where the friction coefficient is explored. Closed-form solutions are compared with experimental results in a comprehensive review in Ref. [11]. Moreover, it suggests that they can be incorporated in numerical tools for efficient fretting fatigue lifetime predictions.

The observations on structures and specimens, as well as the estimations of stresses in fretting problems, illustrate the importance of the plastic strains in these problems. Neuber type formulas can describe the evolution of the plastic strain under certain conditions, but they cannot account for the complex phenomena in fretting fatigue. And therefore, both researcher and engineers rely more and more on complex finite element computations both for the understanding of the phenomena and for the lifetime predictions on structures.[12–17]

In a recent work, Ambrico and Begley[18,19] studied how different cyclic shakedown regimes are reached in the case of a fretting problem defined by a sphere in contact with a plane. They compared the solutions obtained by the finite element method (FEM) using different elastoplastic material behaviours.

Other recent studies[20–22] discuss the microscopic–macroscopic scale effects by conducting elastoplastic computations on a distribution of metallic grains subject to fretting fatigue. An interesting topic discussed in Ref. [21] is the shakedown of the different grains under the cyclic loading and the onset of the plastic strain for fatigue phenomena.

The preceding review illustrates different computational methods to estimate the stress and strain fields in a fretting setup. In order to estimate the lifetime of a structure, one has to adjoin a fatigue analysis to the estimation of the shakedown cycle. The elastic shakedown (ES) theorems for a large class of constitutive models have been recently presented in Ref. [23], which has been extended for different configurations of contact problems in Refs [24–27]. Numerical methods[28–30] have been proposed for the numerical determination of the shakedown cycle in contact problems. However, because of the complex computational structure of these methods, they will not be applied directly in our paper.

Under the assumption of a lifetime defined by a crack initiation, the Dang Van fatigue criterion is one of the successfully applied fretting fatigue criteria.[13,31–33,15,34,12] This multiaxial criterion is based on the shakedown concept and a multiscale homogenisation scheme. Its relation to crack initiation phenomena related to mixed stick–slip regime of fretting was discussed in Refs [32,33]. The multiscale scheme of this criterion was further related to the stress gradient fatigue in Ref. [35] (generated also by the stress configuration in fretting fatigue configuration), but we shall not extend this idea in this paper.

The present paper addresses the problems of the influence of the hardening model (pure kinematic, pure isotropic or combined kinematic and isotropic) on the outcome of a fretting setup. The material parameters used here correspond to an Inconel and a Titanium alloy. The results are discussed in terms of the cyclic shakedown regime, the contact stick–slip regime (introducing a new parameter) and the criticality of the stress state in terms of a Crossland or a Dang Van high-cycle fatigue (HCF) criterion. The computations are performed for a large number of loading parameters expressed as applied normal force, horizontal displacement and friction coefficient. Numerical maps for slip, shakedown and fatigue are automatically generated and analysed.

A COMPLETE COMPUTATIONAL APPROACH FOR LIFETIME ESTIMATION

The analysis presented next shows the point of view of a design engineer who should estimate the lifetime of a given part under a given cyclic loading using a computational model. It is performed in two steps:

- A *mechanical analysis* provides the fatigue loading cycle in the space of the state variables, that is, stresses, strains and plastic strains. This analysis is generally performed using a finite element programme.
- A *fatigue analysis* provides a lifetime estimation for the complete structure. The main assumption of this analysis is that an elastic or PS state is reached in all points of the structure.

This lifetime estimation is based on a fatigue criterion using the limit shakedown cycle computed beforehand as the main input. Ratcheting (RA) is equally a possible outcome of the mechanical analysis but has to be interpreted using specific criteria in the lifetime procedure.

The design engineer is facing a series of constraints such as project duration and computational environment. In order to perform the analysis, he or she has to choose the appropriate modelling, including constitutive and friction laws, boundary conditions and finite element models. The outcome as well as the computational speed of the analysis

will depend on the demanded accuracy. A robust and rapid computational model is therefore necessary. The robustness is defined here in terms of the error in the lifetime associated with the variations in the input parameters.

THE COMPUTATIONAL MODEL

The fretting fatigue configuration studied here is a flat punch with rounded edges sliding on the flat surface of a substrate. The punch is subjected to a controlled vertical force and a horizontal displacement imposed on the upper surface of the pad. The substrate has a length of 20 mm and a height of 10 mm, while the pad has a length of 2.5 mm and has rounded edges with a radius of 0.25 mm. The configuration resembles an experimental fretting fatigue setup developed by MTU to reproduce realistic operational conditions of highly loaded blade–disk attachments as presented in Ref. [12]. This fretting rig will not be discussed in this work. A schematic view of the setup is shown in Fig. 1. The materials used in the experiments are Titanium 64 (Ti64) for the pad, and Inconel 718 (In718) or Titanium 64 for the substrate. Their standard materials parameters are given in Table 1; they match values from material manufacturing databases or from literature as reported, for example, in Refs [36,37]. These materials are usually used in parts of turbomachineries in aeroengines. Both configurations (Ti64 on Ti64 and Ti64 on In718) will be discussed in this paper.

The constitutive law

One of the important choices in a design procedure is the constitutive law of the material. A series of research papers developed sophisticated constitutive laws, which provide a precise description of the softening or hardening behaviour of materials during cyclic loading. A class of such models is given by the constitutive models of the Armstrong–Frederick type as explained in Lemaitre and Chaboche,[38] where one can adjust different hardening behaviours in order to fine-tune the cyclic behaviour of the material. However, one should remark that the computing time is increasing with growing number of hardening models included in the constitutive law. One of the main questions is therefore the complexity that has to be included in the constitutive law in order to observe a desired effect.

In order to have a better understanding of this question, we propose in this work to compare three hardening models associated with a von Mises elastoplastic behaviour, each identified for the two materials under consideration, Titanium and Inconel:

- A *nonlinear isotropic hardening* (denoted as ISO).

The material parameters have been identified from the monotonic traction curve to failure.

- A *linear kinematic hardening* (denoted as KIN).

The material parameters have been identified from the stabilized cycle at midlife and from cyclic material behaviour at imposed strain.

- A *combined isotropic and kinematic hardening* (denoted as COMB).

The material parameters have been identified by a least squares fit from both a monotonic loading and the evolution of the cycles at mid-lifetime.

Figure 2 represents the experimental stress–plastic strain curves and the corresponding calibrated combined

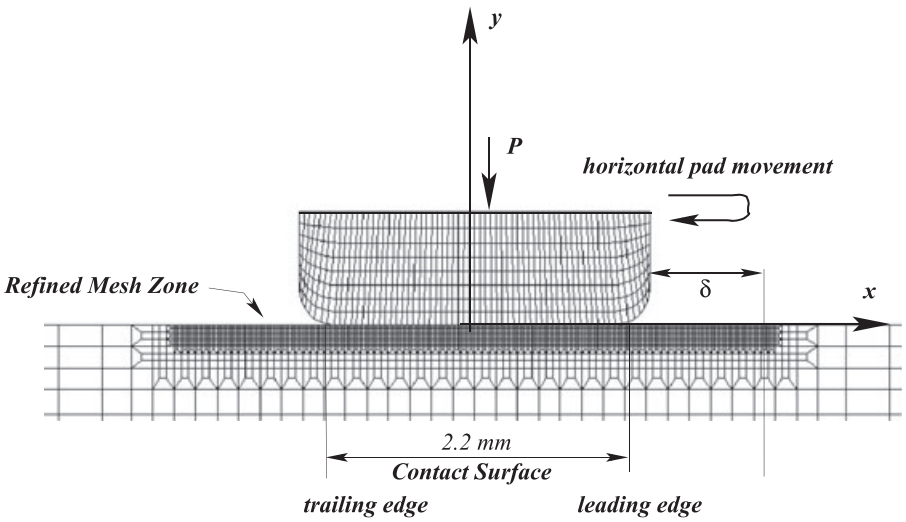

Fig. 1 The finite element model of the setup with a fine mesh of the substrate.

Table 1 Standard material properties for the Inconel 718 and the Ti64 alloys

Material	Young modulus (GPa)	$R_{2\%}$ (MPa)	R_u (MPa)
Inconel 718	208	>1000	>1300
Ti64	114	>800	>900

hardening models for both Inconel 718 and Titanium 64 at room temperature. In both cases, we have represented the monotonic and cyclic response of the material. Both stress and plastic strain axes have been adimensionalized with respect to reference values for confidentiality reasons. For a detailed discussion of rate dependent and independent plasticity models forthe Inconel 718, one can refer to Ref. [39].

Numerical model

The mechanical analysis is performed in 2D plane strain, using the ABAQUS[40] finite element software. The corresponding mesh is displayed in Fig. 1. Four-node linear elements (CPE4I) are used. The contact interaction between the pad and the substrate is realized using the ABAQUS contact pair procedure based on a master–slave algorithm. The tangential contact behaviour is defined by a Coulomb friction model. The pad is considered as purely elastic. The detailed analysis is only performed on the refined region of the substrate mesh placed under the contact zone, where plasticity occurs.

The substrate is defined by 3420 elements and 3593 nodes, with 253 nodes in the potential contact surface (element size of 16 µm). The pad is defined by 508 elements and 603 nodes, with 51 nodes on the contact surface. We have previously used a more refined and converged mesh for the pad and the substrate.[12] The aim here is to perform a parametric study by varying the friction coefficient μ, the normal load P and horizontal displacement δ within the ranges given in Table 2. As 1680 simulations are performed and in order to keep computations in reasonable time, we opted for a coarser mesh, especially for the pad considered as elastic. This is not the case for the substrate that is the object of the analysis in this paper. The element size of the mesh used is compatible with that of the process volume found by Amargier *et al.*[36] or the relevant representative volume element (RVE) used for fatigue life estimation by Wackers *et al.*[12] The accuracy of the refined mesh can be checked in different ways. If the solution remains in the elastic regime, a direct comparison with closed-form solutions proposed for instance in Refs [41–43] can be performed. In the present elastoplastic analyses, we choose an element size of 16 µm, which is of the order of the fatigue RVE size.[36,12]

The boundary conditions are defined by the following: (i) a normal load $-P\underline{e}_y$ and (ii) a reciprocating horizontal displacement varying between 0 and δ along $\underline{e}$ prescribed on the upper surface of the pad ($\underline{e}_x$ and $\underline{e}_y$ are, respectively, unit vectors along the x and y directions, Fig. 1). The normal displacement of these surface nodes is rigidly blocked

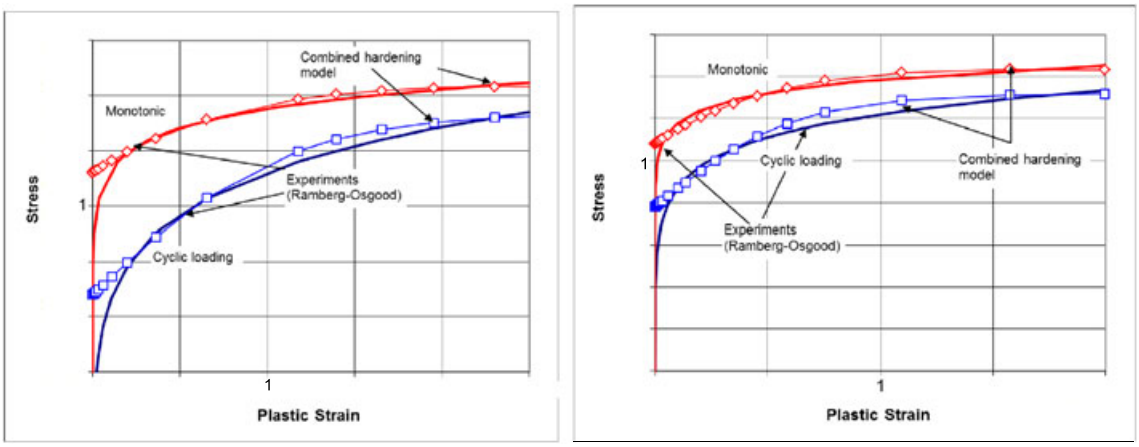

Fig. 2 Experimental stress–plastic strain curves and associated corresponding hardening models for Inconel 718 and Titanium 64 at room temperature (the axes are adimensionalized with respect to reference values, for confidentiality reasons).

Table 2 Ranges of the studied parameters: friction coefficient μ, applied normal load P and horizontal displacement δ

δ (µm)	2.2.	4.4	6.6	8.8	10.	12.	14.	16.	18.	20.		
P (kN)	1.	2.	2.5	3.	4.	5.	6.	7.	7.5	8.	9.	10.
μ	0.1	0.3	0.4	0.5	0.6	0.7	0.8					

Please note that all combinations between the members of the rows have been studied.

in order to eliminate a possible rotation of the pad, as it is the case in a series of experimental fretting setups. On the substrate, the displacements on the faces far from the contact area are rigidly blocked.

The loading is applied for 40 cycles, in order to check if a shakedown state has been numerically reached. The performed analysis showed that, depending on the loading conditions, elastic, PS or RA states can be reached. Although methods are available for the estimation of the nature of long-term behaviour of structures under cyclic loadings,[18,19,44] this number of cycles has been arbitrarily chosen and should not be considered as a standard limit for reaching a shakedown state.

GLOBAL OBSERVATIONS

The classical way to analyse the asymptotic regime (i.e. for a very large number of loading cycles) stems from global experimental observations and requires to plot the tangential force Q against the tangential displacement of the pad δ over all cycles, as represented in Figs 3 and 4. Different kinds of responses are possible: (i) the steady state is a reversible cycle (i.e. a straight line in this case), the regime is non-dissipative and is defined as an ES (Fig. 3). (ii) The steady state is a closed cycle with a nonzero area; this loop indicates energy dissipation and is defined as PS (even if the dissipation may result only from friction). (iii) No closed loop is reached for the tangential force (i.e. its evolution changes cycle after cycle); energy dissipation is equally present, and the regime is denoted as RA (Fig. 4). The split between the energy dissipated in friction and in plastic strain is a difficult task, as well as the precise numerical determination of the frontier between the PS and the RA, or of the stick–slip regime.

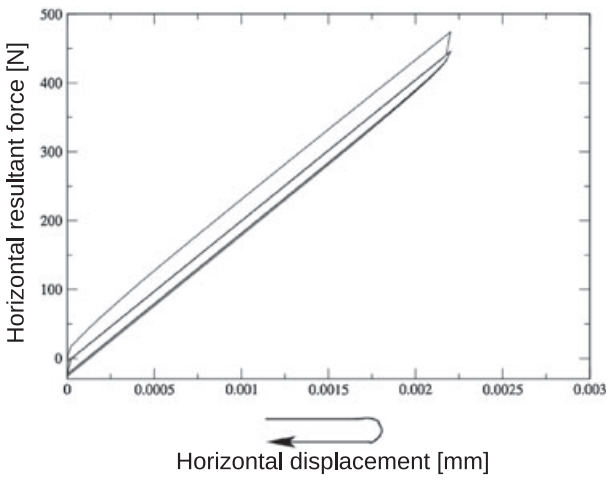

Fig. 3 The global fretting loop, that is, evolution of the force on indenter versus horizontal displacement – elastic shakedown case.

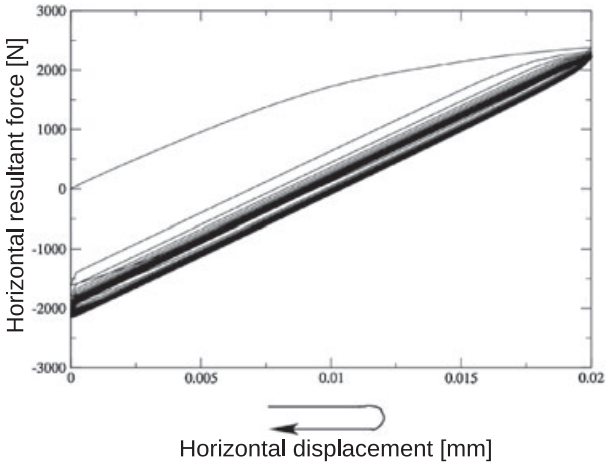

Fig. 4 The global fretting loop, that is, evolution of the force on indenter versus horizontal displacement – ratcheting case.

The disadvantage of these global graphics is that they can only track the global shakedown or slip regimes, and they do not permit to detect the local regimes. The global RA example displayed in Fig. 4 must have several nodes in a RA state. In a similar way, the global ES presented in Fig. 3 has almost all nodes in ES but can still have some elements in PS or RA that are not detected with the global variables.

We shall therefore propose, in the next two sections, several parameters that enable a precise analysis of the shakedown state and the stick–slip regime.

THE SHAKEDOWN STATE

The estimation of the shakedown state has been performed, after 40 loading cycles, for all points of the refined mesh. This zone is placed beneath the contact zone as displayed in Fig. 1. It represents the region where plasticity is localized during the cyclic loading as observed from the distribution of plastic strain (Fig. 5).

In Fig. 6, the evolution of the equivalent plastic strain magnitude (PEMAG) in the case of combined isotropic and kinematic hardening (COMB) is displayed with respect to the number of half cycles for all the nodes in the refined mesh. The chosen computation presents nodes that will have elastic or PS or RA behaviour. This type of representation has been used in order to classify the behaviour of the structure for a given external load. In order to estimate automatically the shakedown state, the definition of Ambrico and Begley[18,19] (slightly modified in Ref. [44] for thermomechanical cases) has been used.

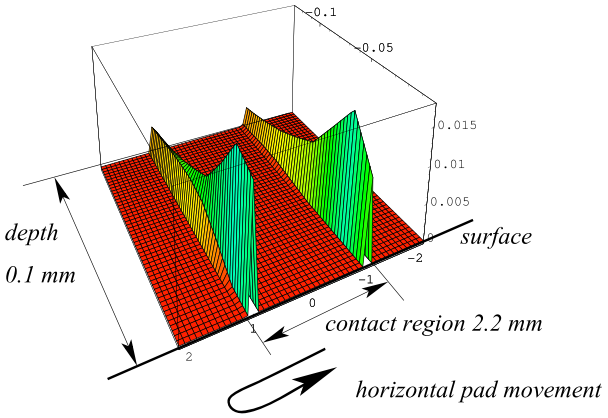

Fig. 5 Typical spatial distribution of the equivalent plastic strain (vertical axis) in the refined part of the mesh after the 40th loading cycles (combined hardening, **P = 7.5** kN, **δ = 12.0 μm** m and **μ = 0.3**).

The RA strain has been defined as the difference in equivalent plastic strain at the last computed time step of two consecutive cycles:

$$\varepsilon_r(i) = \varepsilon_{eq}\left(t_f(i)\right) - \varepsilon_{eq}\left(t_f(i-1)\right) \tag{1}$$

where ε_{eq} is the equivalent plastic strain and $t_f(i)$ denotes the last time step of the cycle i. $\varepsilon_c(i)$, the cyclic strain on the cycle i, is the equivalent strain amplitude computed on each cycle from which the RA component has already been extracted:

$$\varepsilon_c(i) = \left(\max_{t\in[t_i(i),t_f(i)]} \varepsilon_{eq}(t) - \min_{t\in[t_i(i),t_f(i)]} \varepsilon_{eq}(t) \right) - \varepsilon_r(i) \tag{2}$$

The meaning of both variables is graphically illustrated in Fig. 7 on a magnified zone of the preceding Fig. 6.

Another test was equally needed to check whether the structure has reached stabilized limit state, which will be denoted as follows:

- *ES: elastic shakedown* is reached when the cycling and the RA strain on the last cycles are both smaller than a given tolerance dependent of the yield strain:

$$\varepsilon_c(i) < \alpha\varepsilon_Y \qquad \text{and} \qquad \varepsilon_r(i) < \alpha\varepsilon_Y \tag{3}$$

with i the number of the cycle. The parameter α was taken of the same magnitude as in Refs [18,19]: $\alpha \approx 0.007$. $\varepsilon_Y = \sigma_Y/E$ is the yield strain defined as the ratio between the yield limit (stress) and the Young modulus.

- *PS: plastic shakedown* is reached when the RA strain on the last cycles is smaller than a given tolerance dependent of the yield strain:

$$\varepsilon_c(i_f) > \alpha\varepsilon_Y \qquad \text{and} \qquad \varepsilon_r(i_f) < \alpha\varepsilon_Y \tag{4}$$

- *RA: ratcheting* is reached when none of the preceding conditions is met:

$$\varepsilon_c(i_f) > \alpha\varepsilon_Y \qquad \text{and} \qquad \varepsilon_r(i_f) > \alpha\varepsilon_Y \tag{5}$$

Moreover, in order to refine our analysis, we check whether the RA strain ε_r is stabilized at a constant value over the last cycles. The RA is defined as stable if the increase in RA strain on the last cycles is smaller than a given tolerance:

$$\varepsilon_r(i_f) < (1+\beta)\varepsilon_r(i_f - k) \tag{6}$$

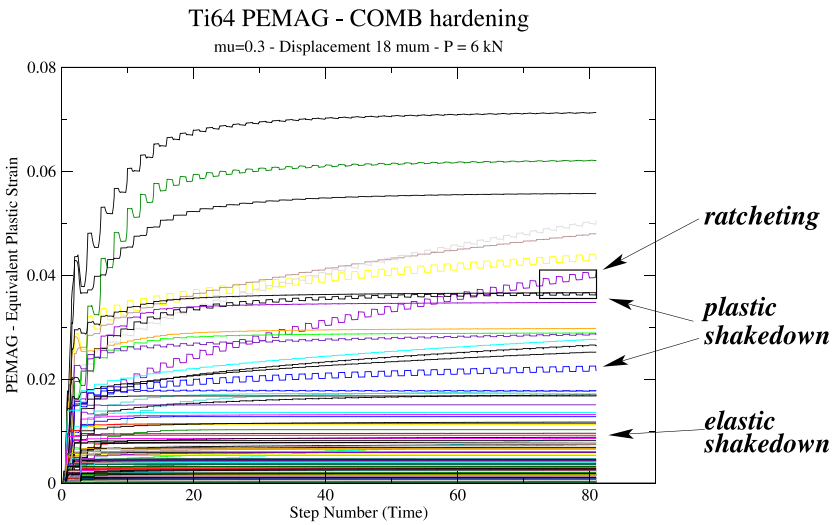

Fig. 6 An evolution of the equivalent plastic strain magnitude (PEMAG) with the number of half cycles in the case of combined isotropic and kinematic hardening (COMB) showing nodes in elastic and plastic shakedown as well as ratcheting. A zoom of the rectangular region is presented in Fig. 7.

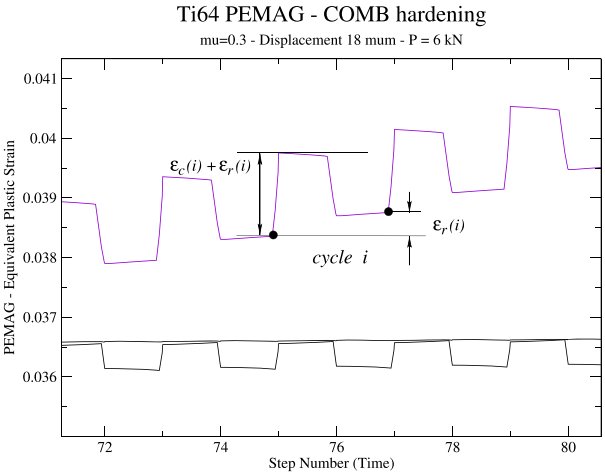

Fig. 7 Zoom of the evolution of plastic strain with number of half cycles and the illustration of the quantities $\boldsymbol{\varepsilon_c(i)}$ and $\boldsymbol{\varepsilon_r(i)}$.

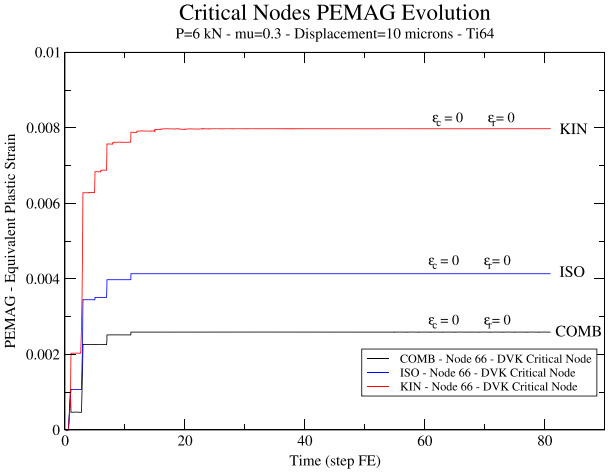

Fig. 8 Evolution of plastic strain in a case of elastic shakedown, for the three different constitutive models (kinematic, KIN; isotropic, ISO; and combined, COMB).

with i_f the last cycle and k a fixed number of cycles to be analysed. The tolerance parameter β represents the percent of RA strain increase that is considered as acceptable for a stabilized computation. The results presented next correspond to $\beta = 0.05$.

Figure 6 displays a large range of behaviours for different nodes of the mesh during the same computation. For each node, the evolution of the equivalent plastic deformation (PEMAG) is plotted as a function of the number of half cycles. It allows to determine the nature of the asymptotic elastoplastic state of the node. When the plastic deformation becomes constant (horizontal line in Fig. 6, stated by the condition Eq. 3), the point experiences ES. When the plastic deformation becomes cyclic (stated by the condition in Eq. 4), the point is in PS. Finally, when it keeps on increasing cycle after cycle (stated by the condition in Eq. 5), the regime is RA. The structure is in an ES, when all its nodes are in ES (the plastic strain reaches a horizontal limit for all nodes, Fig. 8).

We recall that even for the same external loading, the local response will depend on the constitutive law. The level of plastic strain reached for a given node will depend on the constitutive law (see, e.g. in Fig. 8). For each constitutive law, we plot the evolution of the equivalent plastic strain and the corresponding value of ε_c and ε_r at the critical node with respect to Dang Van fatigue criterion. One can only remark that the limit values ε_c and ε_r are different. This result is in accordance with the fact that the strain–stress cycles stabilize in different regions of the space, which will be discussed in the next section.

Starting from the preceding definition of the local shakedown state ES, PS or RA, in each node, we classify a computation as the following:

- *ES: elastic shakedown* when all the nodes are in ES.
- *PS: plastic shakedown* when at least one node is in PS, no node in RA.
- *RA: ratcheting* when at least one is in a RA state.

Using this classification, we have plotted the limit state of the structure as a function of the loading parameters P and δ, as displayed in Fig. 9. The three plots correspond to the three constitutive laws for a friction coefficient $\mu = 0.3$; each plot is based on 120 different computations. This global behaviour has equally been recovered for the other tested friction coefficients. This trend of similar behaviour between the constitutive laws will be later observed in the stick–slip regime and fatigue predictions.

The PS zone seems to be an exception from the rule, as it varied in each case. However, one should recall that the limit state is defined in terms of the tolerance constants α and β and that the variations are really small. In order to better understand the behaviour, we propose to explore a limit case obtained for Ti64, with $P = 6$ kN and $\delta = 18$ μm and $\mu = 0.3$ (Fig. 10).

For each constitutive law, we choose two nodes: the critical nodes in terms of the Dang Van fatigue criterion and in terms of maximal cyclic strain or RA strain. Both critical nodes correspond, in each case, either to the leading or trailing edge of the contact region, where maximal pressure occurs. In the case of an isotropic hardening, an ES state is almost reached. The computation has been classified as PS because of the cyclic strain $\varepsilon_c = 0.001$, which is just over the tolerance.

For the kinematic hardening law, the cycle is at the lower limit of RA case, very close to a PS state, with a RA strain $\varepsilon_r = 0.001$ just over the tolerance value. In the combined hardening, we observe a clear RA case, where the RA node is not the critical node in the sense of the fretting fatigue.

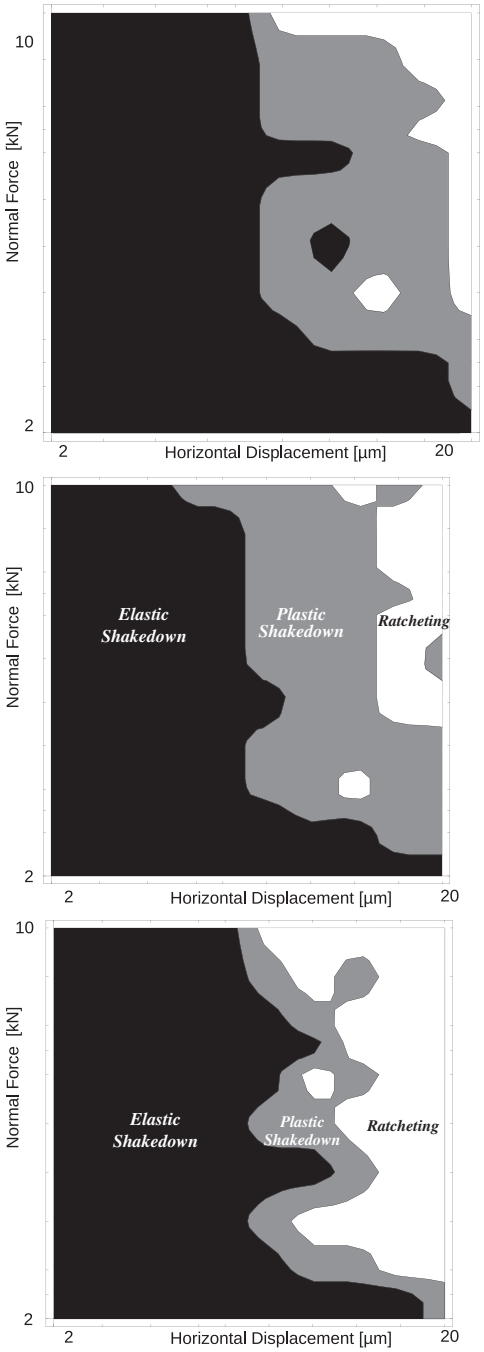

Fig. 9 Shakedown maps for **μ = 0.3** and for the three different constitutive models of Titanium: isotropic hardening (top), kinematic hardening (middle), combined hardening (bottom).

The variations of the limit behaviour might seem troublesome at a first glance. This is related to the tolerances used for the characterization of the limit states, which are very small and easily switch the final response from one case to another one.

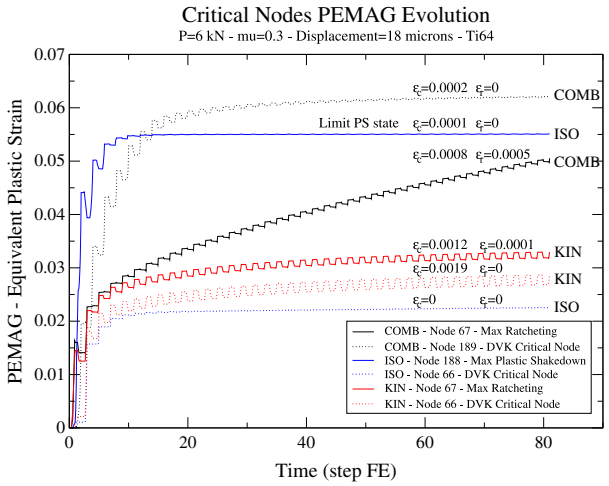

Fig. 10 Evolution of plastic strain in a ratcheting case for the different constitutive models (kinematic, KIN; isotropic, ISO; and combined, COMB) of Ti64.

For the complete range of tested friction coefficients ($\mu \in [0.1,0.8]$), similar patterns of shakedown and RA are obtained for both Inconel 718 and Titanium 64.

STRESS AND STRAIN PATH

In this section, we explore the strain–stress responses of the critical points during the cyclic loading and the nature of the asymptotic regime.

The critical points are located, as already mentioned, at the leading and trailing edges of the active contact zone and correspond to the region of maximal surface pressure. Moreover, the plot of the spatial distribution of equivalent plastic strain in Fig. 5, shows that plasticity is localized on two regions beyond the critical points. In analysing this figure, one should observe the scale difference of depth and the contact region that are displayed using their real aspect ratio in Fig. 1. This pattern of plastic strain distribution has been recovered in practically all computations, independent of the shakedown state, which has been reached and already reported in Ref [5].

As an example of the strain–stress path at the critical nodes, we choose the loadings: $\mu = 0.3$, $P = 6$ kN, $\delta = 6.6$ μm and $\delta = 18$ μm. The loading with an imposed displacement $\delta = 18$ μm was extensively discussed in the previous section, as it provided limit case of PS and RA. The smaller imposed displacement $\delta = 6.6$ μm leads to an ES for all material behaviours. As a first approximation, we can state that the three constitutive laws provide similar amplitudes of the components, but with different mean values.

In the case of $\delta = 6.6$ μm, ES is reached for all hardening laws in a few elastoplastic cycles. In Fig. 11b and d, the limit stress–strain cycles of the critical nodes (numbered 66 and 189) located at the leading and trailing edges of the contact are displayed . They have quite the same amplitudes, even if their mean values are different. This is an expected result. Indeed, in the case of ES, the asymptotic cycle is an elastic response superposed on a time independent residual state. This residual state is due to the plastic deformation induced by the first loading cycles and is therefore dependent on the hardening law. The apparent dispersion of the *xy* stress component is equally because of the graphical representation, where the plot range is an order of magnitude smaller than in the neighbouring plots for the *xx* component.

The case of $\delta = 18$ μm leads, after 40 loading cycles, to a PS for the isotropic hardening, and a RA limit behaviour for the kinematic and the combined hardening. We recall that the isotropic hardening was close to the ES limit and the kinematic one close to the PS limit. In Fig. 12, we present the evolution of the von Mises equivalent shear stress J_2 versus the hydrostatic stress Σ_H.

Comparing the components at the two critical nodes (located at the leading and trailing edges of the contact), a difference between the two points is noticed. This difference is because, as the substrate is elastoplastic, the plastic strain generated in the first half loading cycle creates an asymmetry that could remain, attenuate or completely disappear after application of the following cycles, depending on the parameters of the problem. Indeed, the shear component *xy* keeps track of the slip direction at the edges of the contact zone, while the axial *xx* component is at both ends in compression. One can also remark that there is no clear classification of the constitutive models in terms of created plastic strain, even if the combined hardening seems to create the largest strain in all studied cases.

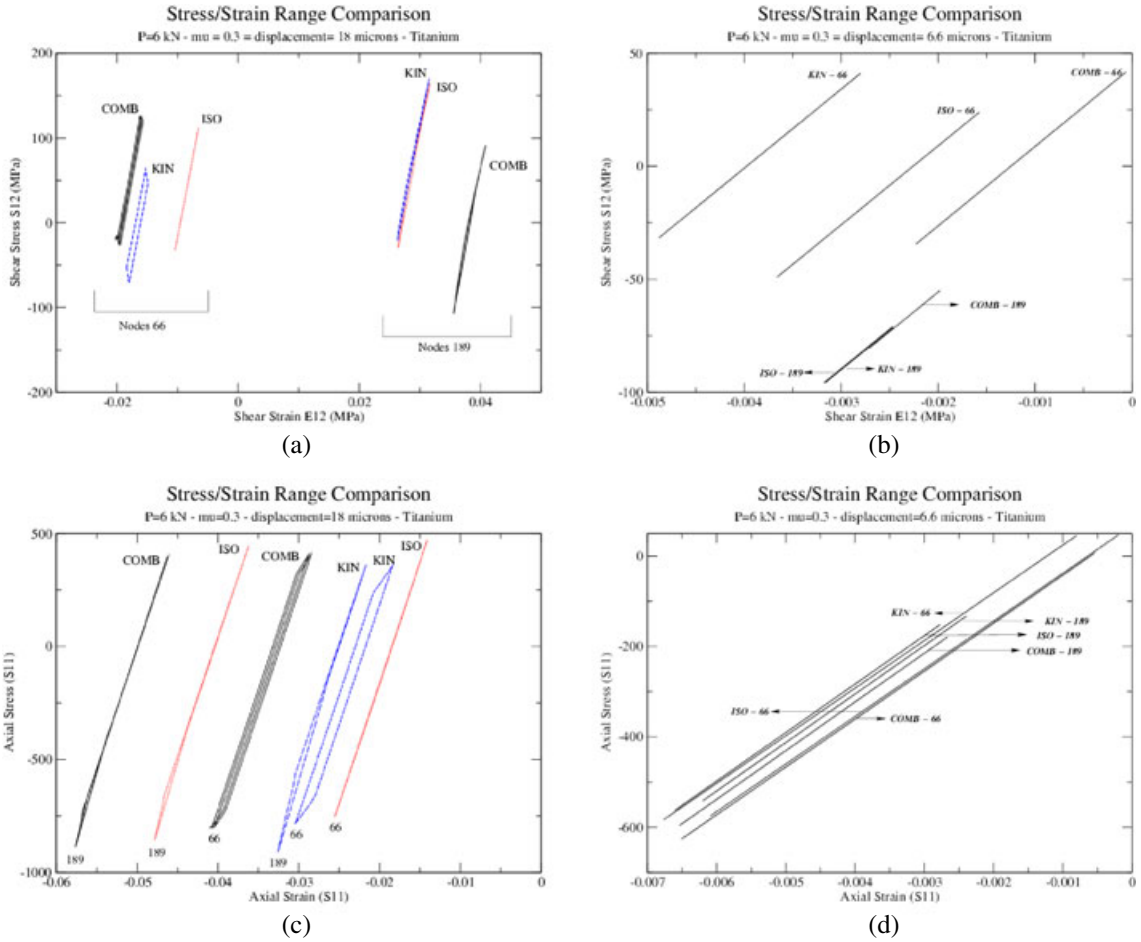

Fig. 11 Comparison of the strain–stress paths in elastic shakedown (b) and (d) and plastic shakedown and ratcheting (a) and (c). Panels (a) and (b) represent the paths in the space of the shear component *xy*, and panels (c) and (d) represent the paths for tangential surface component *xx*. The paths correspond to the critical nodes (numbered 66 and 189) at the leading and trailing edges of the contact zone.

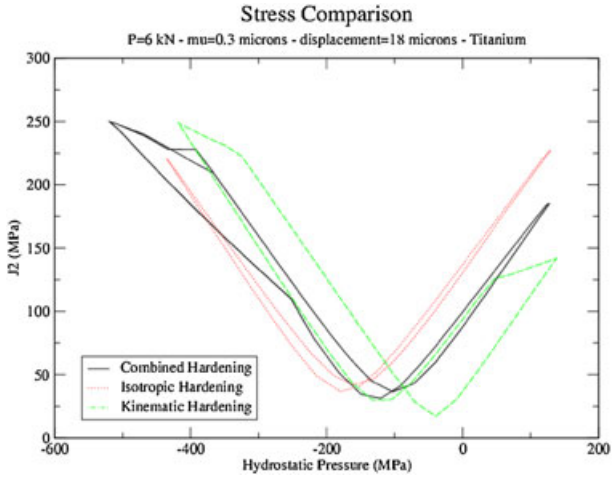

Fig. 12 Comparison of the stress path in terms of $\mathbf{J_2}$ and $\mathbf{\Sigma_H}$, that is, von Mises equivalent shear stress and hydrostatic stress at the critical nodes for the three constitutive laws in the case of Titanium.

Finally, we can state that the reported patterns have been observed both for Inconel and Titanium.

THE STICK–SLIP REGIONS AND REGIMES

It is a well accepted fact that the contact regime either full-stick, stick–slip or full-slip has capital effect on the fatigue behaviour. One can estimate the contact regime for each point and each time step, by using FEM computations. However, the obtained information is cumbersome, and it is therefore interesting to find a practical way to monitor and to plot the evolution of the contact regime with increasing time. Our proposal can be summarized in the following way.

We recall that a Coulomb friction law is assumed for the contact:

- $q < \mu |p|$ for a point in *stick* and
- $q = \mu |p|$ for a point in *slip*.

p and q are the contact pressure and shear (in a two dimensional computation):

$$p = n \cdot \sigma \cdot n \qquad q = t \cdot \sigma \cdot n$$

where n and t denote, respectively, the unit normal and tangent vector to the surface.

Using the values of p and q provided directly by the FEM computation, we check whether a node is in slip or stick using these definitions. From a practical view, slip is assumed when $q > 0.99\mu |p|$. To visualize the contact regime at each time instant, we associate, in a graph, a pixel at every contact point: *black* for a stick and *white* for slip regime (Fig. 13). The vertical axis of the plot is indexed with respect to the computed time instants.

The computations, performed with the parameters given in Table 2, show contact regimes ranging from full-stick to full-slip. Gross slip has not been examined as it corresponds to surface wear. As examples, Fig. 13 displays two plots of different cases: one in full-slip regime (for $P = 2.5$ kN, $\mu = 0.1$ and $\delta = 11.0$ μm) and the other in stick–slip regime (for $P = 2.5$ kN, $\mu = 0.3$ and $\delta = 6.6$ μm).

It is important to remark that in the full-slip regime, the surface is, at some instants, in stick and at other instants in full-slip. The apparition of stick is inevitable at certain instants during a cyclic loading as the change of direction in the applied displacements requires a complete stop of the pad. When increasing imposed horizontal displacement for given P and μ, the regime goes from full-stick to a partial slip regime. The partial slip regime occurs at almost all time instants. This usual behaviour has been observed for all computations on

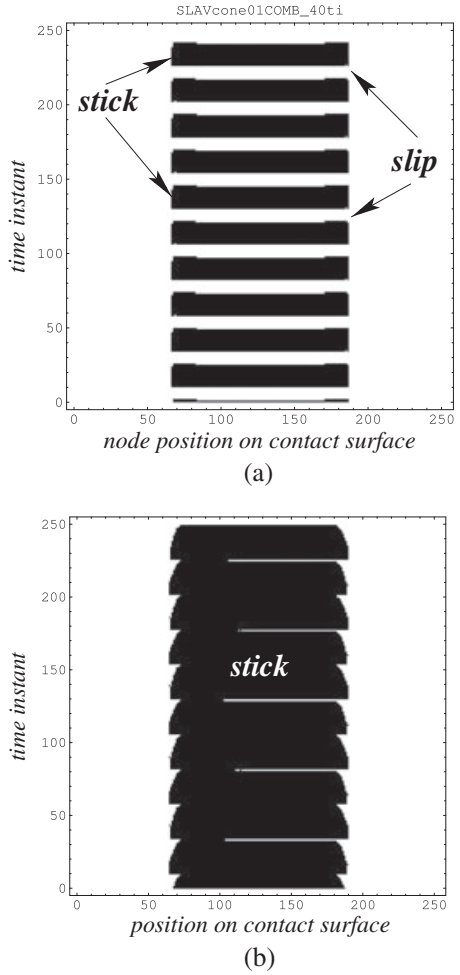

Fig. 13 Stick–slip Plot for Ti64-combined hardening: (a) $\mathbf{P = 2.5}$ kN, $\boldsymbol{\mu = 0.1}$ and $\boldsymbol{\delta = 11}$ **μm** and (b) $\mathbf{P = 2.5}$ kN, $\boldsymbol{\mu = 0.3}$ and $\boldsymbol{\delta = 6.6}$ **μm** (1 cycle = 6 time instants).

both Titanium and Inconel independently of the chosen hardening model. The apparition and the length of the slip zone will however depend on the loading parameters.

In Fig. 14, for the loading parameters $P = 6$ kN, $\delta = 18$ μm and $\mu = 0.6$, the distribution of pressure and shear in the contact area is plotted for two time instants corresponding respectively to the middle of the fretting cycle (maximal and displacement of the pad) and the end of the fretting (zero displacement of the pad). One can remark that the pressure peak at the trailing edge of the pad is higher than the other one, explaining why the slip region occurs asymmetrically starting at the leading edge of the pad. This matches the observations of the plastic strain, which is higher at the trailing edge of the pad. Therefore, the trailing edge will exhibit more frequently PS or RA than the leading edge. This fact has equally been observed in recent experiments.[45]

In order to better estimate the remarkable property that there is not important differences between the three hardening models tested, we shall next propose a measure of the slip region during a computation. The new variable will be called *global slip percentage* and is defined by the percentage of surface in slip with respect to the total surface:

$$s_g = \max_t s_s(t)/s_c(t) \tag{7}$$

where $s_s(t)$ is the area of the surface slip at time t and $s_c(t)$ the area of the surface in contact. Note that this quantity has a different meaning than the sliding criterion (%GS) introduced by Heredia and Fouvry[46] to estimate the proportion of cycles in gross slip in a fretting test.

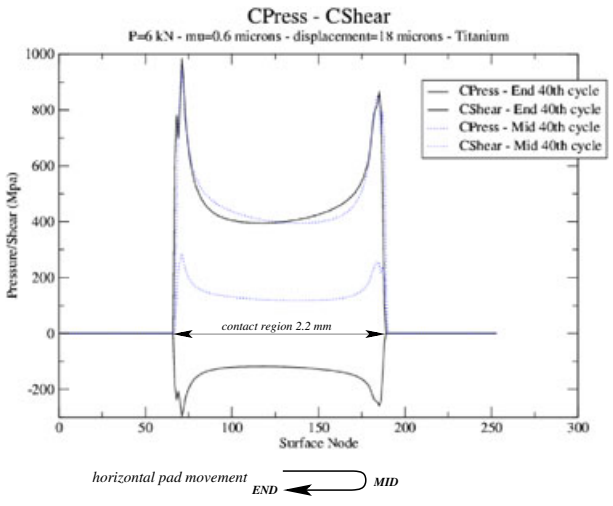

Fig. 14 Surface pressure and shear distribution on the contact region displayed for the time instants at the middle and at the end of the fretting cycle (maximum and zero displacements, respectively).

When this definition is applied to the cases plotted in Fig. 13, we obtain the following estimations: for $\delta = 6.6$ μm and $s_g = 0.40$, and for $\delta = 20.0$ μm and $s_g = 0.74$.

It is obvious that the global slip percentage will be a function of the applied load and the constitutive law of the material. In order to compare the slip behaviour of the different constitutive laws, we propose to plot the global slip percentage as a function of the applied horizontal displacement δ and vertical load P: $s_g(\delta,P)$. A usual result is displayed in Fig. 15 for Titanium modelled with combined hardening and a friction of $\mu = 0.3$. Similar observations are made for all computed friction coefficients with Titanium or Inconel material. However, one should not forget that the frontiers of the stick and the full-slip domains will vary with the friction coefficient. For example, in the explored region, we practically do not encounter stick for low friction coefficients such as $\mu = 0.1$ and do not encounter full-slip for high friction coefficient such as $\mu = 0.8$, which matches the practical experience.

We can conclude by generally stating that there were less than 15% of difference in slip between the different models. The global pattern is stabilized after a few number of cycles if ES in attained in the computation and does not evolve in an important manner even if PS or RA are reached. When interpreting these results, one should fully understand that the explored range of imposed displacements is rather small and that slip generally occurs only at the trailing edge of the pad.

FATIGUE PREDICTIONS

In the previous sections, we analysed the results of the fretting computations from the point of view of the shakedown state and the stick–slip zone. In this section, we use these results to estimate lifetimes, understood as macroscopic crack nucleation times.

The fatigue crack initiation criterion can be defined in a generalized framework as a local relation between the limit mechanical state under the cyclic loading and the number of cycles to failure. A classical form for the fatigue criterion is

$$\max_x \varphi(\underline{x}, \underline{\underline{\sigma}}, \underline{\underline{\varepsilon}}, \underline{\underline{\varepsilon}}^p, \ldots) N_f^\beta = c$$

where $\underline{x}$ is the point of the structure under consideration and $\underline{\underline{\sigma}}, \underline{\underline{\varepsilon}}, \underline{\underline{\varepsilon}}^p, \ldots$ denote the history over a cycle of the stresses, strains, plastic strains and other internal variables, respectively. N_f is the number of cycles to failure, and β and c are two material parameters to be calibrated from independent experiments.

In the present case, we are mainly interested in the HCF domain. This option is justified by a range of the chosen parameters, the small fretting displacement δ and the applied normal force P. Let us recall that in the 'infinite' life domain of HCF, structures are in an ES state at the macroscopic and mesoscopic scale, while in the finite life domain, they are subjected to plastic or RA loading at least at the mesoscopic scale. In these two regimes, most of the fatigue criteria are therefore based on the macroscopic stresses.

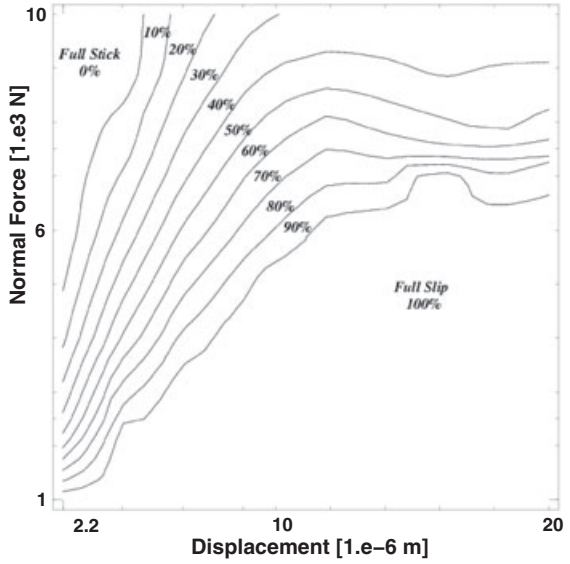

(a)

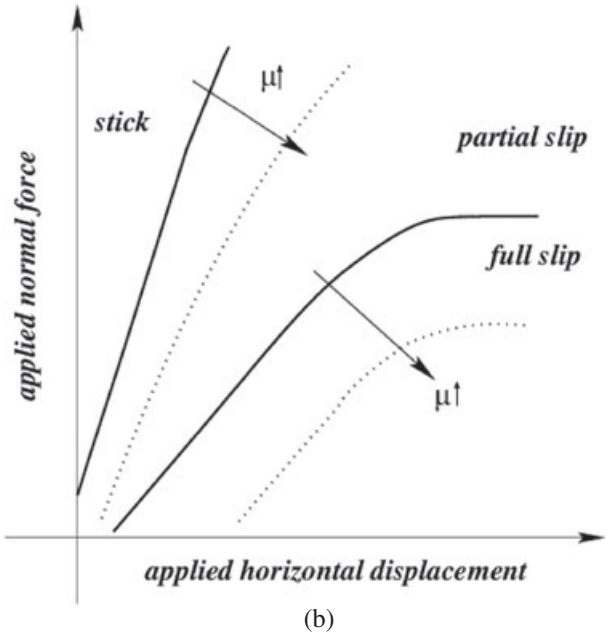

(b)

Fig. 15 Slip map for a friction coefficient $\mu = 0.3$: (a) for a combined hardening and (b) a schematic view.

Our choice was to analyse the results using Crossland and Dang fatigue criterion we shortly present in the following.

The *Crossland fatigue criterion* can be defined under the generalized form:

$$\sqrt{J_{2,a}} + a_N^1 \max_t \Sigma_H(t) < b_N^1 \tag{8}$$

where $\sqrt{J_{2,a}}$ is the amplitude of the deviatoric stress path in the von Mises norm and $\Sigma_H = \mathrm{tr}\,\underline{\underline{\sigma}}/3$ the hydrostatic stress. a_N^1 and b_N^1 denote two material parameters calibrated to predict the crack initiation after N loading cycles. We recall that the initial Crossland criterion was defined for $N = \infty \approx 10^6$ cycles.

In a similar way, the *Dang Van fatigue criterion* can be defined under the generalized form:

$$\max_t(\tau(t) + a_N \Sigma_H(t)) < b_N \tag{9}$$

where τ is the mesoscopic shear and Σ_H is the hydrostatic stress. a_N and b_N denote two material parameters calibrated to predict the crack initiation after N loading cycles.

The Dang Van fatigue criterion has been established for the prediction of *the fatigue limit* (infinite lifetime). It is essentially on the basis of the concept of ES at both macroscopic and mesoscopic scales of the structure.[47] It has been largely used in fretting fatigue analyses.[13,31–33,15,34,12]

It is important to notice that both the classical Crossland and Dang Van criteria can be applied to a structure only when the structure is macroscopically in ES. The preceding section has clearly demonstrated that this is not always the case for the chosen loads of this study. However, as they are defined only in terms of the stress path, we can consider them as a fatigue criticality measure of the stress path.

The Dang Van criticality (DVK) is defined as the normalized distance from the critical mesoscopic stress path to the fatigue limit line by:

$$\mathrm{DVK} = \max_t \frac{(\tau(t) + a_N \Sigma_H(t)) - b_N}{b_N - a_N \Sigma_H(t)} \tag{10}$$

and similarly, the Crossland criticality (CROS) by:

$$\mathrm{CROS} = \frac{\sqrt{J_{2,a}} + a_N^1 \max_t \Sigma_H(t) - b_N^1}{b_N^1 - a_N^1 \max_t \Sigma_H(t)} \tag{11}$$

A general trend is observed which is that plasticity and damage are located near the surface at both edges of the contact zone, with, however, the trailing edge suffering the highest damage. The lifetime is always diminishing

with increasing imposed displacement. This is consistent with experimental observation in Ref. [2]. The increase of lifetime arrives only in the gross slip regime, which is not explored in this work. The lifetime first decreases and then increases with increasing friction coefficient. The imposed normal load does not influence the lifetime for small imposed displacements, whereas for large displacements, a larger load corresponds to a smaller lifetime.

Some stress loading paths in the Dang Van diagram are shown in Fig. 16, and the distribution of DVK along the surface is plotted in Fig. 17. One can remark that the general shape is practically hardening independent. However, the levels of the pressure spikes at the leading and trailing edges of the contact zone may vary within 15–20%. Moreover, we can equally observe that the spike

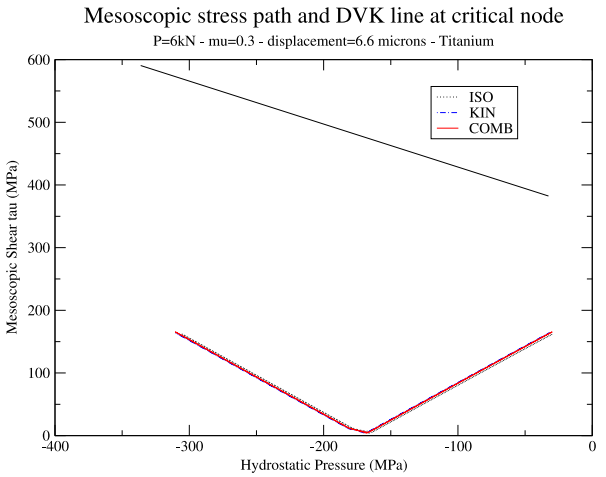

Fig. 16 Stress path in terms of mesoscopic shear ($\boldsymbol{\tau}$) and hydrostatic stress (p) for the three hardening models: (a) for $\boldsymbol{\delta} = 6.6\,\boldsymbol{\mu}$m, $\boldsymbol{\mu} = 0.3$ and $P = 6$ kN and (b) for $\boldsymbol{\delta} = 18\,\boldsymbol{\mu}$m, $\boldsymbol{\mu} = 0.3$ and $P = 6$ kN. (The straight lines represent the fatigue limit for the Dang Van criterion).

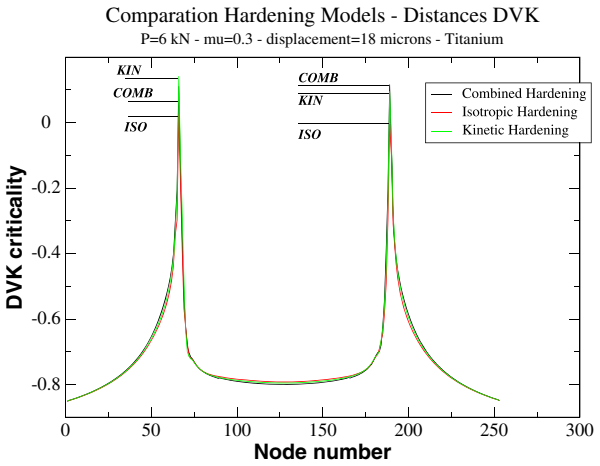

Fig. 17 Dang Van criticality along the surface – comparison between the different hardening models.

is generally higher at the leading edge than at the trailing one, which is in accordance with experimental observations.

In Fig. 18, the DVK has been plotted for the different hardening laws and a fixed friction coefficient $\mu = 0.3$ in Fig. 18. The axes of the plot are the applied horizontal displacement δ and normal force P for $\mu = 0.3$. One can remark that the global shape is hardening independent and that the values of criticality vary within a 15% range between the laws.

However, not all the considered regions in Fig. 18 are in ES as already discussed in the preceding sections. In Fig. 19, we present the elastic PS and RA zones in terms of applied loads for the same friction coefficients $\mu = 0.3$ and compared them with the region where the Dang Van criterion predicts fatigue. One can first remark that the trends observed for the three constitutive laws are quite similar. The differences are a slight shift in the frontiers corresponding to variations of the loading parameters of about 10%.

The computed maps (Figs 18 and 9) show a similar shape and are consistent, for the three different constitutive behaviours. Moreover, they reproduce the expected behaviour from experiments. In order to continue our analysis, we overlap the fatigue criticality and the shakedown maps (Fig. 19). One can remark that, on the one hand side, we obtain a region, at low imposed displacements, where ES dominates and fatigue criticality is negative, meaning infinite lifetime is expected. On the other hand side, we obtain a region, at high imposed displacements, where RA or PS overlap a positive fatigue criticality, meaning that a finite lifetime is to be expected. Both regions are consistent with fatigue experimental observations.

Let us now analyse the boundary zone delimiting the preceding zones. This region experiences PS or RA while its fatigue criticality is negative, meaning infinite lifetime; this is in contradiction with experimental facts and Dang

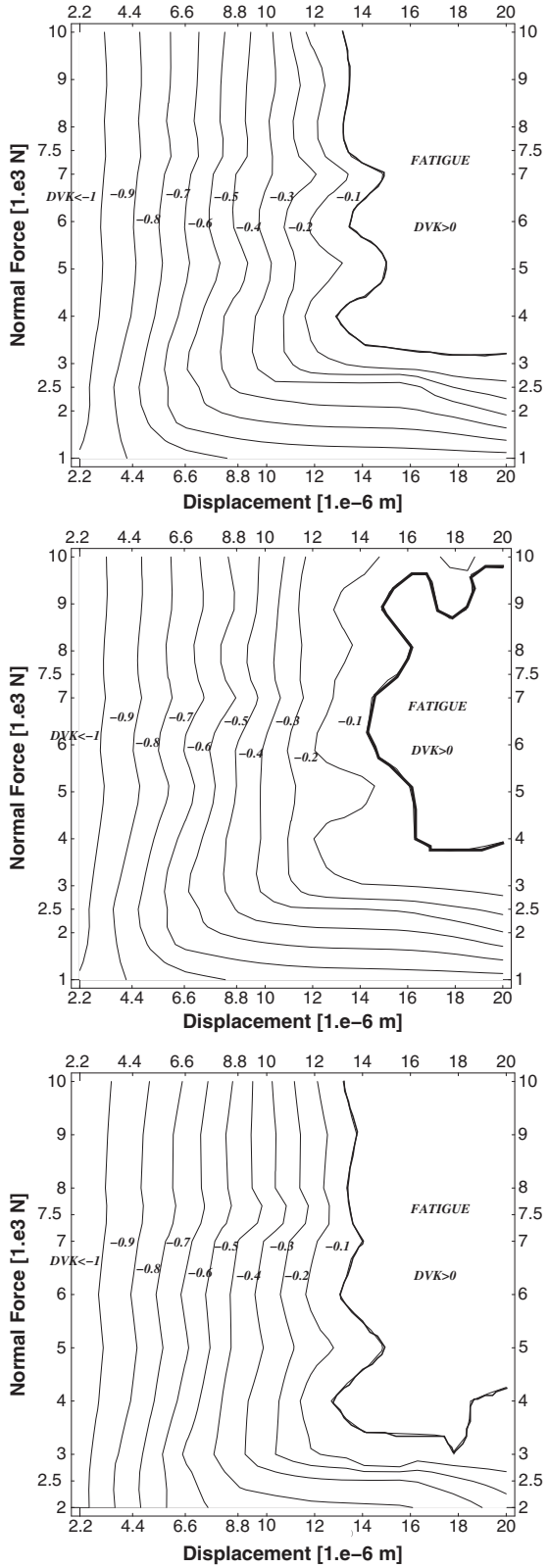

Fig. 18 Contours plots of the Dang Van criticality for $\mu = 0.3$ and for the three different constitutive models of Titanium: isotropic hardening (top), kinematic hardening (middle) and combined hardening (bottom).

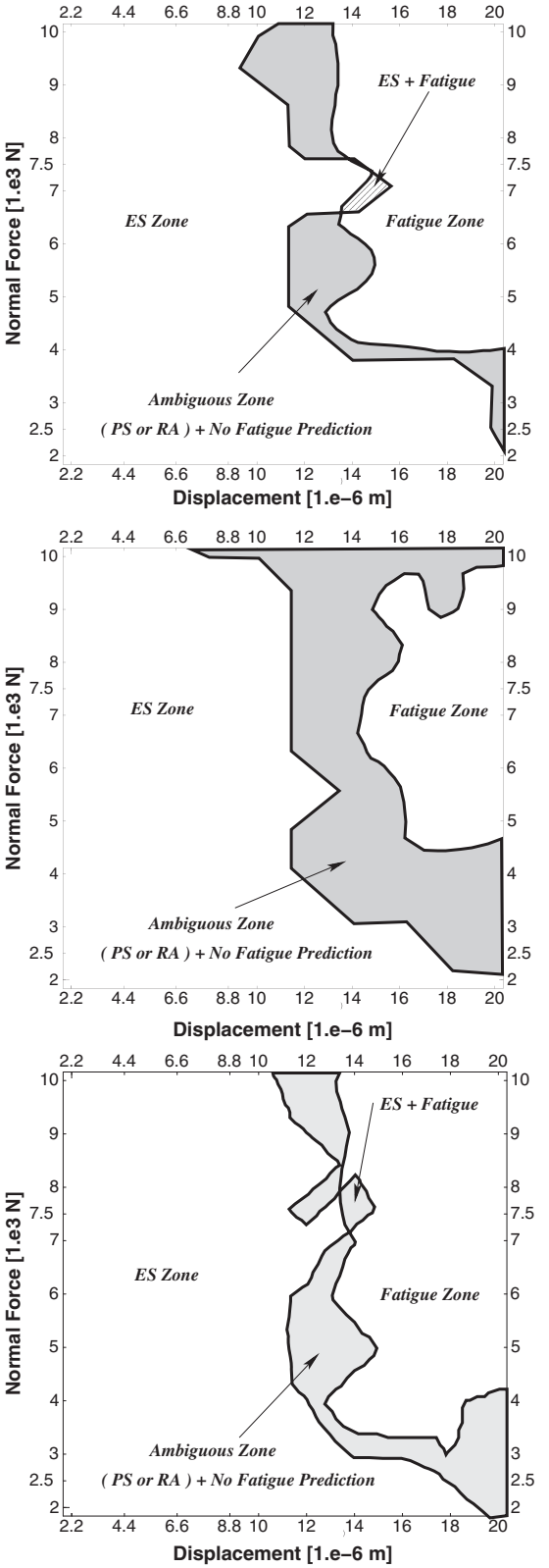

Fig. 19 Theoretical domain of applicability of the Dang Van criterion (ES, i.e. elastic shakedown domain) versus predicted fatigue domains for Titanium: isotropic hardening (top), kinematic hardening (middle), combined hardening (bottom).

Van fatigue concepts.[47–49] Moreover, one can equally remark that the zone has a weird border, which is difficult to accurately assess.

Several arguments can be proposed for the outcome of the overlapping: the choice of the fatigue criterion and its application or the definition of the shakedown zones. It is obvious that a more precise meshing would lead to higher stresses and therefore modify the negative criticality region or that a change in the tolerance parameters of shakedown analysis could move the border between elastic and PS or RA.

We shall not propose a solution to remove this ambiguity in this paper. However, it is important to note that care must be exercised in matching the maps and choosing parameters and tolerances in the computations. The final judge will, as always, be a comparison with some experimentally obtained fretting maps.

CONCLUSION

In this paper, we have explored the possibility of creating fretting, shakedown and fatigue map from a series of computations. The computations were performed on a particular configuration of a fretting rig (a rounded flat punch made of Ti64 on the flat surface of a substrate made of In718 or Ti64) and used three constitutive behaviours and a large range of parameters (normal force, tangential displacement and friction coefficients).

The analysis was based on an automatic detection of shakedown regime, as initially proposed in Refs [18,19] and the Dang Van or the Crossland multiaxial fatigue criterion as a measure of damage. The chosen parameters ranges permitted to attain various contact conditions (from full-stick to full-slip) and limit states (from ES to RA).

The computations showed that different maps can be obtained by the parametric computations and that their outcome is, as expected, close to the global trends observed in experimental studies. The three considered hardening models lead to similar results in terms of slip zones, ES and damage. Therefore, for design purpose's, if a combined hardening model is not available, a model with an isotropic or kinematic hardening model can be accepted. However it is important to understand that the quantitative results are equally dependent of the tolerance parameters defining the shakedown regime and a specific study should be performed before applying the results in a engineering design procedure. If one questions the appropriate hardening model to be used for a specific material configuration, we would recommend to take as an input not only the material behaviour but also to analyse the predicted results also in terms of expected shakedown regime and slip area. This result is consistent with those obtained by Dick *et al.*[22] and Goh *et al.*[21] who showed that RA is more likely to occur near the contact surface by using more refined viscoplastic material models including global and crystal plasticity.

The fatigue predictions obtained using the Dang Van or the Crossland criterion predict as expected the same critical points, at the edges of the contact zone. The results are models independent up to 10%, in terms of their values. When applying fatigue criteria for industrial design purpose, it is appropriate to adapt the criteria. The computations presented here are based on a hot-spot like approach associated with an element size. However, taking into account the important stress concentrations, a volumetric or gradient type approach permits to better represent the reality and distribute the local load on a RVE.

As a final conclusion, we can state that maps for the lifetime prediction of fretting fatigue problems can be generated from finite element computations. Their global shape of the map is robust with respect to the computational parameters. However, it has been noted that care must be exercised in matching the fine details of the computations with experimental results in order to achieve a good prediction. Several questions remain to be answered by future studies, as for example, (i) correlation between the elastoplastic computations and more direct elastic analysis (including different asymptotic models), (ii) fine tuning of the tolerances defining the shakedown regimes, and (iii) transitions between infinite and finite lifetime and the shakedown regime in different loading regions.

Acknowledgements

The authors gratefully acknowledge the financial support for this project from the German Federal Ministry of Economy (framework Lufo3) and the French National Research Agency (project Fast3D-ANR-11-BS09-012-0).

REFERENCES

1 Waterhouse, R. B. (1981) Fretting Fatigue. Applied Science Publishers, London.
2 Vingsbo, O. and Soderberg, S. (1988) On fretting maps. *Wear*, **126**, 137–147.
3 Zhou, Z. R., Nakazawa, K., Zhu, M. H., Maruyama, N. Kapsa, P., and V., L. (2006) Progress in fretting maps. *Tribol. Int.*, **39**(10):1068–1073.
4 Shinde, S. and Hoeppner, D. W. (2005) Quantitative analysis of fretting wear crack nucleation in 7075-t6 aluminum alloy using fretting maps. *Wear*, **259**(1–6):271–276.
5 Johnson, K. L. (1987) Contact Mechanics. Cambridge University Press, Cambridge, UK.
6 Nowell, D. and Hills, D. A. (1990) Crack initiation in fretting fatigue. *Wear*, **136**, 329–343.
7 Hills, D. A. Sackfield, A. and Dini, D. (2005) The finite and semi-infinite tilted, flat but rounded punch. *Int. J. Solids Struct.*, **42**, 4988–5009, 9.

8 Hills, D. A. Nowell, D. and Dini, D. (2006) Recent developments in the understanding of fretting fatigue. *Eng. Fract. Mech.*, **73**, 207–222, 1.
9 Ciavarella, M. (2006) Some observations on the clna model in fretting fatigue. *Tribol. Int.*, **39**, 1142–1148.
10 Szolwinsky, M. P. and Farris, T. N. (1996) Mechanics of fretting fatigue crack formation. *Wear*, **198**, 93–107.
11 Hills D. A., Thaitirarot A., Barber J. R., and Dini D. (2012) Correlation of fretting fatigue experimental results using an asymptotic approach. *Int. J. Fatigue*, **43**, 62–75.
12 Wackers, P., Arrieta, V., Alquezar-Getan, M., Constantinescu, A. and Maitournam, H. (2010) A modeling approach to predict fretting fatigue on highly loaded blade roots. *J. Eng. Gas Turbines Power*, **132**, 082101.
13 Petiot, L., Vincent, L., Dang Van, K., Maouche, N., Foulquier, J. and Journet, B. (1995) An analysis of fretting-fatigue failure combined with numerical calculations to predict crack nucleation. *Wear*, **181-183**, 101–111.
14 Calcaterra, J. and Naboulsi S. (2005) Design methodology to investigate contact fatigue damage in turbine engine hardware. *Int. J. Fatigue*, **27**, 1133–1141, 9.
15 Arrieta, V., Wackers, P., Dang Van, K., Constantinescu, A. and Maitournam, H. (2004) Modelling attemps to predict fretting fatigue life in turbine components.
16 Wavish, P. M., Houghton, D., Ding, J., Leen, S. B., Williams, E. J. and McColl, I. R. (2009) A multiaxial fretting fatigue test for spline coupling contact. *Fatigue Fract. Eng. Mat. Struct.*, **32**, 325–345.
17 Zhu, Y., Kang, G., Ding, J. and Zhu, M. (2013) Study on bending fretting fatigue of lz50 axle steel considering ratchetting by finite element method. *Fatigue Fract. Eng. Mat. Struct.*, **36**, 127–138.
18 Ambrico, J. M. and Begley, M. R. (2000) Plasticity in fretting contact. *J. Mech. Phys. Solids*, **48**, 2391–2417.
19 Ambrico, J. M. and Begley, M. R. (2001) The role of macroscopic plastic deformation in fretting fatigue life predictions. *Int. J. Fatigue*, **23**, 121–128.
20 Mayeur, J. R., McDowell, D. L. and Neu, R. W. (2008) Crystal plasticity simulations of fretting of ti-6al-4v in partial slip regime considering effects of texture. *Comput. Mater. Sci.*, **41**, 356–365.
21 Goh, C.-H., McDowell, D. L. and Neu, R. W. (2006) Plasticity in polycristalline fretting fatigue contacts. *J. Mech. Phys. Solids*, **54**, 340–367.
22 Dick, T. and Cailletaud, G. (2006) Fretting modelling with a crystal plasticity model of ti6al4v. *Comput. Mat. Sci.*, **38**, 113–125.
23 Nguyen, Q. S. (2003) On shakedown analysis in hardening plasticity. *J. Mech. Phys. Solids*, **51**, 101–125.
24 Antoni, N. and Nguyen, Q. S. (2008) Shakedown theorems in contact mechanics. *Comptes Rendus de l'Académie des Sciences Mécanique*, **336**, 341–346.
25 Antoni, N., Nguyen, Q. S. and Ragot, S. Slip-shakedown analysis of a system of circular beams in frictional contact. *Int. J. Solids Struct.*, **45**, 5189–5203, 2008.
26 Klarbring, A., Ciavarella, M. and Barber, J. R. (2007) Shakedown in elastic contact problems with coulomb friction. *Int. J. Solids Struct.*, **44**, 8355–8365.
27 Dini, D., Sackfield, A. and Hills, D. A. (2005) Comprehensive bounded asymptotic solutions for incomplete contacts in partial slip. *J. Mech. Phys. Solids*, **53**, 437–454.
28 Maitournam, M. H., Benjamin, P. and Thomas, J. J. (2002) Determination of the asymptotic response of a structure under cyclic thermomechanical loading. *Comptes Rendus Mécanique*, **330**, 703–708.
29 Peigney, M. and Stolz, C. (2003) An optimal control approach to the analysis of inelastic structures under cyclic loading. *J. Mech. Phys. Solids*, **51**, 575–605.
30 Spiliopoulos, K. V. and Panagiotou, K. D. (2012) A direct method to predict cyclic steady states of elastoplastic structures. *Comput. Meth. Appl. Mech. Eng.*, **223-224**, 186–198.
31 Fouvry, S., Kapsa, P., Vincent, L. and Dang Van, K. (1995) An analysis of fretting-fatigue failure combined with numerical calculations to predict crack nucleation. *Wear*, **195**, 21–24.
32 Maouche, N., Maitournam, M. H. and Dang Van, K. (1997) On a new method of evaluation of the inelastic state due to moving contacts. *Wear*, **203–204**, 139–147.
33 Dang Van, K. and Maitournam, H. (2000) On a new Methodology for Quantitative Modeling of Fretting Fatigue. Book Series: American Society for Testing and Materials Special Technical Publication, **1367**, 538–552. http://www.astm.org
34 Araujo, J. A., Nowell, D. and Vivacqua, R. C. (2004) The use of multiaxial fatigue models to predict fretting fatigue life of components subjected to different contact stress fields. *Fatigue Fract. Eng. Mater. Struct.*, **27**, 967–978.
35 Bertolino, G., Constantinescu, A., Ferjani, M. and Treiber, P. (2007) A multiscale discussion of fatigue and shakedown for notched structures. *Theor. Appl. Fract. Mech.*, **48**, 140–151.
36 Amargier, R., Fouvry, S., Chambon, L., Schwob, C. and Poupon, C. (2010) Stress gradient effect on crack initiation in fretting using a multiaxial fatigue framework. *Int. J. Fatigue*, **32**, 1904–1912.
37 Lillamand, I., Barrallier, L., Lalanne, B. and Castex, L. (2001) Cyclic modelling of the mechanical state produced by shot-peening. *Fatigue Fract. Eng. Mater. Struct.*, **24**, 93–104.
38 Lemaitre, J. and Chaboche, J. L. (1990) Mechanics of Solid Materials. Cambridge University Press, Cambridge, UK.
39 Becker, M. and Hackenberg, H. P. (2011) A constitutive model for rate dependent and rate independent inelasticity. application to {IN718}. *Int. J. Plast.*, **27**, 596–619.
40 Getting started with ABAQUS. ABAQUS Inc., 2007.
41 Sackfield, A., Mugadu, A. and Hills, D. A. (2002) The influence of an edge radius on the local stress field at the edge of a complete fretting contact. *Int. J. Solids Struct.*, **39**, 4407–4420.
42 Dini, D. and Nowell, D. (2004) Flat and rounded fretting contact problems incorporating elastic layers. *Int. J. Mech. Sci.*, **46**, 1635–1657.
43 Ciavarella, M., Hills, D. A. and Monno, G. (1998) The influence of rounded edges on indentation by a flat punch. *Proc. Inst. Mech. Eng. Part C J. Mech. Eng. Sci.*, **212**, 319–327.
44 Benoit, A., Maitournam, M. H., Rémy, L. and Oger, F. (2012) Cyclic behaviour of structures under thermomechanical loadings: application to exhaust manifolds. *Int. J. Fatigue*, **38**, 65–74.
45 Cadario, A. and Alfredsson, B. (2006) Fretting fatigue experiments and analyses with a spherical contact in combination with constant bulk stress. *Tribol. Int.*, **39**, 1248–1254.
46 Heredia, S. and Fouvry, S. (2010) Introduction of a new sliding regime criterion to quantify partial, mixed and gross slip fretting regimes: correlation with wear and cracking processes. *Wear*, **269**, 515–524.
47 Constantinescu, A., Dang Van, K. and Maitournam, M. H. (2003) A unified approach for high and low cycle fatigue based on shakedown concepts. *Fatigue & Fract. Eng. Mater. Struct.*, **26**, 561–568.
48 Jabbado, M. and Maitournam, M. H. (2008) A high-cycle fatigue life model for variable amplitude multiaxial loading. *Fatigue & Fract. Eng. Mater. Struct.*, **31**, 67–75.
49 Bosia, S. and Constantinescu, A. (2012) Fast time-scale average for a mesoscopic high cycle fatigue criterion. *Int. J. Fatigue*, **45**, 39–47.